metals

MDPI

Article

Microstructure and Mechanical Properties of an Al-Li-Mg-Sc-Zr Alloy Subjected to ECAP

Anna Mogucheva * and Rustam Kaibyshev

Laboratory of Mechanical Properties of Nanostructured Materials and Superalloys, Belgorod State University, 85 Pobedy, Belgorod 308015, Russia; rustam_kaibyshev@bsu.edu.ru

* Correspondence: mogucheva@bsu.edu.ru; Tel.: +7-4722-58-54-17

Academic Editor: Soran Birosca

Received: 31 August 2016; Accepted: 17 October 2016; Published: 25 October 2016

Abstract: The effect of post-deformation solution treatment followed by water quenching and artificial aging on microstructure and mechanical properties of an Al-Li-Mg-Sc-Zr alloy subjected to equal-channel angular pressing (ECAP) was examined. It was shown that the deformed microstructure produced by ECAP remains essentially unchanged under solution treatment. However, extensive grain refinement owing to ECAP processing significantly affects the precipitation sequence during aging. In the aluminum-lithium alloy with ultrafine-grained (UFG) microstructure, the coarse particles of the S_1-phase (Al_2LiMg) precipitate on high-angle boundaries; no formation of nanoscale coherent dispersoids of the δ'-phase (Al_3Li) occurs within grain interiors. Increasing the number of high-angle boundaries leads to an increasing portion of the S_1-phase. As a result, no significant increase in strength occurs despite extensive grain refinement by ECAP.

Keywords: aluminum alloys; equal channel angular pressing; thermomechanical processing; microstructure; mechanical properties; precipitation

1. Introduction

The formation of a ultra-fine grained (UFG) microstructure through severe plastic deformation (SPD) is an advanced approach to produce semi-finished products from aluminum alloys with a high strength and endurance limit, good ductility and sufficient fracture toughness [1]. It was postulated [1] that the enhanced strength of aluminum alloys is attributed to structural strengthening due to the formation of a UFG microstructure that was defined as a homogeneous and reasonably equiaxed microstructure with average grain sizes of less than ~1 μm; the fraction of high angle boundaries (HAGBs) is higher than 56%. From a practical point of view, a UFG structure can be easily produced in aluminum alloys by equal channel angular pressing (ECAP) [1]. This technique can be scaled up fairly easily for the fabrication of high-volume billets with commercially viable dimensions [1–4].

Most high-performance aluminum alloys are age-hardenable. Precipitation strengthening is a dominant strengthening mechanism for these alloys. It is obvious that only the combination of grain size strengthening with precipitation hardening can significantly affect the strength of these aluminum alloys. The formation of a UFG microstructure significantly affects the size of second-phase precipitations and their distribution within the aluminum matrix [5–10]. Therefore, mechanical properties of age-hardenable aluminum alloys subjected to ECAP depend critically on the aging response including precipitation kinetics and sequence, origin of dispersoids and the precipitate morphology.

Unfortunately, despite numerous studies [11–15] dealing with the examination of extensive grain refinement through ECAP on mechanical properties of these precipitation-hardened aluminum alloys, the effect of a UFG microstructure on precipitation sequence under post-deformation aging is relatively poorly known [5,9,16–18]. It was shown that the formation of a UFG microstructure changes the

precipitation sequence: stable phases precipitate on high-angle boundaries [5] or even within the aluminum matrix [6] that suppresses the appearance of a metastable phase. It is well-known that the strength of an age-hardenable aluminum alloy is a function of grain size strengthening, dislocation strengthening and precipitation hardening. The last strengthening mechanism is most important for this type of aluminum alloy; decrease in the precipitation strengthening due to lack of uniform distribution of metastable phases with coherent or semi-coherent interface boundaries could not be compensated by the two other strengthening mechanisms. As a result, the achievement of increased yield stress (YS) in age-hardenable aluminum alloys is not a trivial task. A positive effect of ECAP on YS is reported in a limited number of studies [5,7–9,17,19,20]. It is worth noting that in all these works the temperature of final aging was lower in comparison with aging temperature used to achieve optimal YS in their coarse grained (CG) counterparts. The low aging temperature was used to prevent over-aging due to precipitations of stable phase coarse particles; application of conventional aging temperature to ECAP processed aluminum alloys leads to rapid softening [9,21].

ECAP Processing of Age Hardenable Aluminum Alloys

Currently, there exist four different routes of thermomechanical processing (TMP) through ECAP for achieving high strength in age hardenable bulk aluminum alloys (Figure 1). First, aluminum alloys usually belonging to 6XXX series are subjected to ECAP at $T \leq 100$ °C in fully annealed [22] or quenched [23,24] conditions without any subsequent artificial aging [22–24] (Figure 1a); post-ECAP natural aging usually occurs at room temperature. An increase in YS varies from ~25% [13] to ~40% [23] in comparison with values specified for these commercial alloys [17]. It seems that an increase in YS is attributed to a combination of dislocation strengthening attributed to low temperature ECAP with solid solution strengthening or precipitation strengthening attributed to natural aging. However, a remarkable reduction in ductility [22–24] is the main disadvantage of this TMP route.

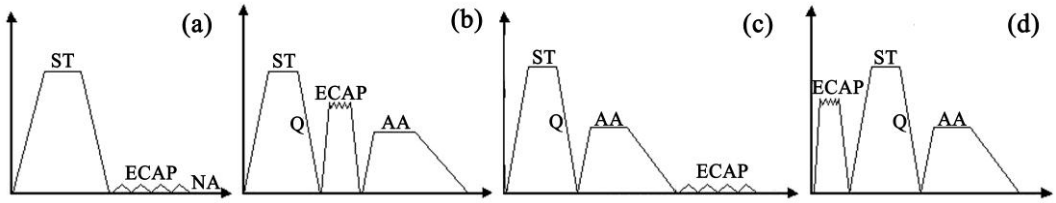

Figure 1. Scheme of thermomechanical treatment. ST—solution treatment, ECAP–equal channel angular pressing, NA—natural aging, Q—Quenching, AA—artificial aging. (**a**) ECAP between ST and NA; (**b**) ECAP between ST and AA; (**c**) ECAP after ST and AA; (**d**) ECAP before ST and AA.

Second, an aluminum alloy in a condition of supersaturated solid solution produced by initial water or oil quenching is processed by ECAP at a temperature below, equal to or slightly higher than the aging temperature (Figure 1b). Finally, the processed alloy is subjected to artificial aging [6–9,17,19,21,25–27]. This is the most popular TMP route. It was found that this route results in the 18%–40% increase in YS. High YS originated from a combination of dislocation strengthening and dispersion strengthening. However, the total elongation decreases by almost a factor of two [6–9,17,21,26,27]. Decreased ductility is attributed to low work-hardening rate [6]. There exists no potential for further work-hardening after this TMP. As a result, uniform elongation does not exceed 3%–5% [7,17]. It was shown that it is possible to increase strength by ECAP with ductility remaining essentially unchanged [19]. However, even in this case, the uniform elongations in an Sc modified AA7055 aluminum alloy subjected to T6 heat treatment were much larger (~15% vs. 2%–3%) in comparison with the material subjected to ECAP processing. It seems that low value of uniform elongation is the main disadvantage of age-hardenable aluminum alloys processed through this route.

Third, aluminum alloys can be subjected to ECAP in aged condition (Figure 1c) [5]. Under ECAP, the mobile lattice dislocation cuts off dispersoids of a metastable phase with semi-coherent or/and

coherent boundaries that leads to their gradual fragmentation into nanoscale particles. The last are thermodynamically unstable due to high surface energy [5]. As a result, a complete dissolution of this particle occurs. Next, the Genie-Preston Zones (GPZ) form providing an increase in hardness [5]. This TMP route is very exotic.

It is worth noting that these three routes of TMP are not viable to produce true grains entirely delimited by HAGBs. Therefore, the deformed structure resulting from these TMP routes could not be interpreted in terms of UFG structure [1]. Careful inspection of structural characterization data [6,8,9,17,19,23,26] showed that, for the most part, crystallites evolved under ECAP are delimited by low-angle boundaries (LAGBs); under SPD, the lattice dislocations arrange into cells and LAGBs or form the dislocation network within initial grains [17]. Therefore, it is not obvious that the grain size strengthening is important for significant increase in YS of aluminum alloys subjected to ECAP through the three aforementioned TMP routes.

Only the fourth route (Figure 1d) of TMP, which was initially developed to process Al-Li alloys [16,28], provides the formation of UFGs entirely delimited by HAGBs. In this route, the post-ECAP standard heat treatment consisting of solution treatment, quenching and final aging can be applied to the aluminum alloy with UFG structure. A critical condition for viability of this method is the stability of UFG structure under solution treatment. Materials such as AA5091 [28], in which abnormal grain growth in UFG structure occurs under solution treatment, are not suitable for this processing method. The fourth route of TMP can be applied to materials such as Weldalite (AA2X95) alloy [16], in which normal grain growth took place; increase in grain size under solution treatment is insignificant. Therefore, it is reasonable to apply the fourth route of TMP only to Sc-bearing aluminum alloys, in which coherent Al_3Sc dispersoids effectively suppress the migration of HAGBs under conditions of solution treatment that retains a UFG structure evolved under prior ECAP [2,29,30]. It was found that a 9% increase in YS of Al-Li alloys processed through this TMP route could be achieved [16]. Concurrently, a 50% increase in ductility and uniform elongation takes place due to the formation of UFG structure and elimination of precipitation-free zones [16].

Thus, the positive effect of UFG structure on mechanical properties of precipitation-hardened aluminum alloys can be achieved only in certain cases:

(I) a UFG structure evolved during ECAP processing must be stable under solution treatment;
(II) aging of a material with UFG structure must be capable to provide significant precipitation hardening.

Accordingly, the present work was conducted to evaluate the feasibility of applying the fourth route of TMP to an Al-Li-Mg-Sc-Zr alloy (designated in Russia as 1421Al). It was shown previously [31] that ECAP at 300 °C of this alloy provides the formation of the well-defined subgrain structure (ε~2), partially recrystallized structure (ε~4) and fully recrystallized structure (ε~8). The last structure is uniform with an average grain size of ~1 μm [2,29–31]; most of the crystallites are true grains entirely outlined by HAGBs. This structure is essentially stable under annealing at a temperature of 450 °C [2,30,32]. Therefore, this alloy can be subjected to solution treatment followed by quenching with a UFG structure. In contrast [29], the partially recrystallized structure in the 1421Al could be unstable under conditions of solution treatment. The 1421Al was developed for application as a structural material for airframes [33]. As a result, the feasibility to use this material is dependent on a combination of strength, toughness and fatigue resistance. From this point of view, it is quite reasonable to examine mechanical properties of the 1421Al in all of the aforementioned structural states; we initially expected that the partially recrystallized structure provides the highest toughness, and the 1421Al with a fully recrystallized structure would exhibit the highest strength. Thus, the aim of this study is to examine the effect of ECAP followed by conventional hardening heat treatment on strength and ductility of this material.

In context of this goal, the effect of post-deformation heat treatment on structure will be examined. In addition, the aging response of the 1421Al with different deformation structure will be analyzed

in relationships with its mechanical properties, which are highly dependent on dispersion of the secondary phase precipitated under aging [33].

The precipitation sequence is indicated in the 1421Al by [33]:

$$SSSS \rightarrow \delta'(Al_3Li) \rightarrow S_1(Al_2LiMg). \quad (1)$$

High strength is provided by precipitation of coherent the δ'-phase dispersoids with an average size of 6 nm [33,34]; high volume fraction of the δ'-phase is a prerequisite condition for achieving the highest strength in the 1421Al. Accordingly, it is very important to dissolve whole Li into solid solution under solution treatment. Next, Li must precipitate in the form of the metastable δ'-phase under aging. Precipitations of the incoherent equilibrium S_1-phase lead to material softening because the amount of Li available for the formation of the δ'-phase in solid solution decreases. The S_1-phase tends to precipitate on HAGBs [35]. Under certain conditions, the precipitations of the S_1-phase can almost suppress the formation of the δ'-phase [33,35]. This leads to a minor strengthening increment by precipitation hardening during aging. It is worth noting that the aging behavior of Al-Li-Mg alloys with a grain size higher than 6 μm is well-known [35]. However, aging behavior of an Al-Li-Mg alloy with UFG microstructure has never been examined.

2. Materials and Methods

The details of the chemical composition of the 1421Al, fabrication procedure and experimental techniques were reported elsewhere [2,32]. It is necessary to additionally report the following. ECAP of samples cut from hot extruded bar [32] was carried out in isothermal conditions at 325 °C using a die with a rectangular shape of channel cross-section [2,32]. The samples strained up to ε~2 and ε~4 were rotated by 90° around the *z*-axis in the same direction and by 180° around the *x*-axis between each pass, i.e., the modified route B_{CZ} [1] was used. The samples strained up to ε~8 were rotated by 180° around the *x*-axis. The pressing speed was approximately 3 mm/s. Next, the samples were subjected to solution treatment at 460 °C followed by oil quenching. Part of these samples was additionally aged at 120 °C for 6 h. Structural characterizations were only performed on samples subjected to post-ECAP or post-hot extrusion heat treatment.

Misorientations were determined using a FEI Quanta 200 3D SEM (FEI company, Hillsboro, OR, USA) fitted with an automated indexing of electron back scattering diffraction (EBSD) pattern collection system provided by EDAX (Mahwah, NJ, USA). Notably, thick and thin lines on the EBSD maps indicate the HAGBs ($\geq$15°) and LAGBs (2°–15°), respectively. Terms "grain" and "subgrain" are used for definition of crystallites, which are entirely delimited by HAGBs and LAGBs, respectively [31]. Term "(sub)grain" is used for definition of crystallites which are bounded partly by LAGBs and partly by HAGBs [31]. Thin foils were examined using a Jeol-2100 (Tokyo, Japan) transmission electron microscope (TEM) with a double-tilt stage and equipped with energy dispersive spectrum analysis (EDS) produced by Oxford Instruments, Ltd. (Oxfordshire, UK) at an accelerating potential of 200 kV. The dislocation density was estimated by counting the individual dislocations within (sub)grain interiors using a method, which is described in previous work [22] in detail, on at least six arbitrary selected typical TEM images for each sample.

Tensile specimens of 6 mm gauge length and 1.4 × 3 mm^2 cross-section were machined from the plates or initial extruded bar [32] with tension axis lying parallel to the last *x*-axis (Figure 2). Both types of samples were subjected to final T6 heat treatment or without heat treatment. These samples were tensioned to failure at ambient temperature at an initial strain rate of 5.6×10^{-3} s^{-1} using an Instron 5882 testing machine (Instron Ltd., Norwood, UK).

Precipitation sequence was examined using a SDT Q600 TA differential scanning calorimeter (DSC) (New Castle, PA, USA) where the specimens after the oil quenching were heated at rates of 10 K/min from 20 °C to 490 °C.

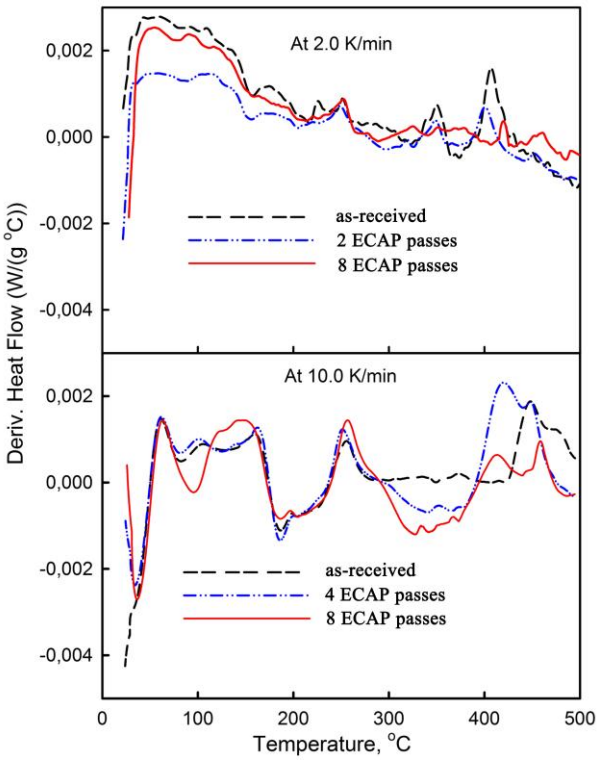

Figure 2. Differential scanning calorimeter thermograms of the solution-treated 1421 alloy at different heating rates.

3. Results

3.1. DSC Analysis

The DSC results are shown in Figure 2. For initial extruded 1421Al and this alloy subjected to ECAP up to total strains of ~2 and ~4, four exothermic peaks at ~60 °C, 90 °C–140 °C, 140 °C–170 °C and 230 °C–280 °C appear during the DSC scan. Therefore, the aging sequence Equation (1) is proposed.

The second and third exothermic peaks are usually attributed to precipitations of the δ′-phase and S_1-phase [33], respectively. It is worth noting that precipitation reactions in the 1421Al subjected to ECAP are shifted to lower temperatures. In contrast, the 1421Al subjected to ECAP up to a total strain of ~8 shows one exothermic peak at 120 °C–180 °C. This peak can be interpreted in terms of precipitation of S_1-phase. However, it is necessary to keep in mind that these DSC experiments are merely indications, and they cannot prove or disprove the formation of different phases.

3.2. Microstructure after Extrusion and Heat Treatment

Hot extrusion resulted in partially recrystallized microstructure in the 1421Al alloy (Figure 3a,b). Coarse grains with dimensions of ~171 and ~21 μm in longitudinal and transverse directions, respectively, are elongated toward the extrusion axis (Figure 3a) after final heat treatment. Chains of recrystallized grains having equiaxed shape and an average size of ~5 μm are located along separate initial HAGBs (Figure 3a). The portion of LAGBs is approximately 54%. It is worth noting the relatively high portion of HAGBs of 46% associated with mainly longitudinal initial boundaries. A well-defined subgrain structure was observed within highly elongated grains (Figure 3c); lattice dislocation density ($\rho \sim 4.5 \times 10^{13}$ m^{-2}) is not so high (Figure 3c). Three different types of secondary phases were found after the T6 heat treatment. Coherent dispersoids of Al_3(Sc,Zr)-phase with an average size of ~20 nm and equiaxed shape are uniformly distributed within grain interiors [31,32]. Particles of the S_1-phase with an average size ranging from ~0.5 to ~0.7 μm and equiaxed shape are predominantly located

on HAGBs or LAGBs (Figure 3c). In addition, coarse particles of the S_1-phase with an average size ranging from ~2 to ~4 μm comprise chains along extrusion axis [32]. Thus, bimodal size distribution of the S_1-phase particles takes place in the 1421Al in hot extruded conditions. Volume fraction of the S_1-phase is ~2 pct. Evidence for a dispersion of very fine coherent δ′-particles with a size of ~5 nm was found due to the TEM study at high magnification (Figure 3d). These particles exhibit specific contrast because the shear modulus of the δ-phase is less than that of the aluminum matrix, and, as a result, coherent stress induces lattice distortion within the soft dispersoids rather than in the strong matrix [33,34]. Thus, this structure is characterized by relatively low dislocation density, large grain size and high volume fraction of the δ′-phase.

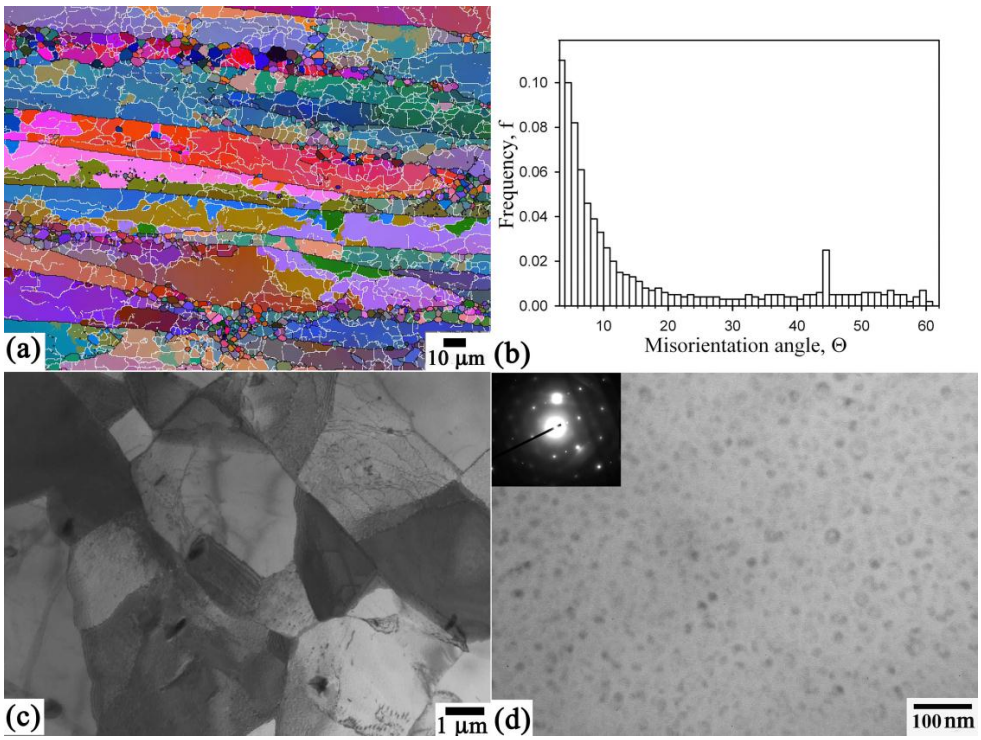

Figure 3. Typical microstructures of the 1421Al as-received and after standard heat treatment: (**a**) misorientation map; (**b**) distribution of misorientations; (**c**) transmission electron microscope (TEM) image of structure; and (**d**) δ′-phase particles (TEM).

3.3. Microstructure after ECAP and Heat Treatment

After ε~2, a partially recrystallized microstructure can be observed (Figure 4a,b). The formation of this structure after a relatively low total strain compared with work [31] is aided by the use of initially extruded billet, a plate shape of samples and an optimal deformation temperature. Areas of grains with an average size of ~1 μm and (sub)grains alternate with areas of subgrains (Figure 4a). The second structure component is dominant. Volume fraction of true grains is relatively low (~20%). The portion of HAGBs is ~55%, and average misorientation is ~18° (Figure 4b). Grains and (sub)grains exhibit essentially equiaxed shape (the aspect ratio (*AR*) is ~1.25). In contrast, subgrains are elongated along the last extrusion direction; dimensions of subgrains in longitudinal and transverse directions are ~3.7 and ~2 μm, respectively (*AR* is ~1.9). The volume fraction of the S_1-phase is approximately 5%, and their size is the same as in the initial hot extruded state after aging (Figure 4e). Coarse particles of the S_1-phase with an average size ranging from ~2 to ~4 μm comprise chains along extrusion axis (Figure 4) as in the hot extruded condition. Particles of the S_1-phase located at triple junctions and on HAGBs are dominant (Figure 4e). However, these particles could be observed in separate grains; most HAGBs are free from the particles of the S_1-phase. A high density of dispersoids of the δ′-phase with

an average size of ~6 nm was found within grain interiors (Figure 4f). No δ′-phase was found near coarse particles of the S_1-phase. Relatively high density of lattice dislocations (ρ~6 × 10^{14} m^{-2}) was observed. The number of dislocations within subgrain structure is higher than that within grains by a factor of ~4. It is worth noting that evidence for grain boundary dislocation was found. Therefore, high temperature annealing did not lead to their adsorption by grain boundaries [35]. Thus, this structure is characterized by high dislocation density, moderate grain size and moderate density of the δ′-phase.

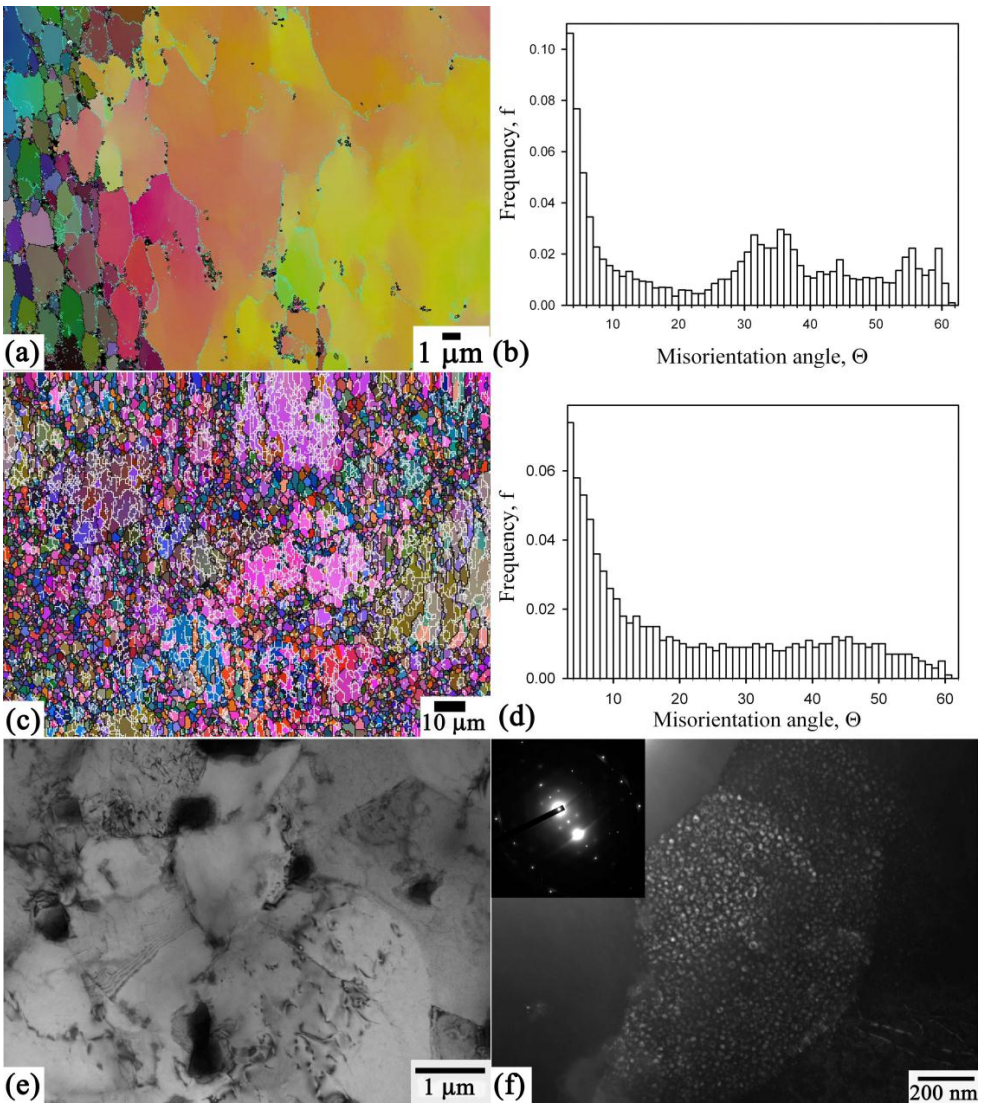

Figure 4. (**a**,**c**) Electron back scattering diffraction maps showing the high and low angle boundaries (dark and light lines, respectively) and boundary misorientation histograms (**b**,**d**) for the 1421Al alloy deformed by equal-channel angular pressing to strains of (**a**,**b**) 2; (**c**,**d**) two and standard heat treatment; and (**e**,**f**) transmission electron microscope image of structure ε~2 and standard heat treatment.

Pressing to a strain of ε~4 results in a recrystallized structure, the portion of unrecrystallized grains, which are highly elongated along the last extrusion direction, is minor (Figure 5a,b). The fraction of recrystallized grains with an average size of ~1 μm is very high, ~90%. It seems that the effect of annealing under solution treatment on this UFG is insignificant. It seems that the structure evolved during ECAP remains nearly unchanged. The population of HAGBs is ~82%; the average misorientation is 31° (Figure 5a,b). There exists a large difference in dislocation density within crystallites. True grains contain a low dislocation density (ρ~4 × 10^{13} m^{-2}), whereas high dislocation

density of (ρ~1 $\times$ 10^{15} m^{-2}) is observed within (sub)grains and unrecrystallized grains. The formation of recrystallized structure strongly affects the origin and distribution of precipitations. S_1-phase particles with a size ranging from 0.2 to ~0.4 μm are uniformly distributed within areas of fine grains. S_1-phase particles are located on HAGBs and even within grain interiors (Figure 5e). It is worth noting that well-defined shells of unknown origin can be observed around S_1-phase particles (Figure 5e), In addition, coarse S_1-phase particles are also uniformly distributed within the aluminum matrix (Figure 5). Their overall volume fraction attains ~16%. There is weak evidence for the appearance of dispersions of the δ'-phase within micron scale grains (Figure 5f); their volume fraction is negligible. Thus, this structure is characterized by moderate dislocation density, UFG structure and low density of the δ'-phase.

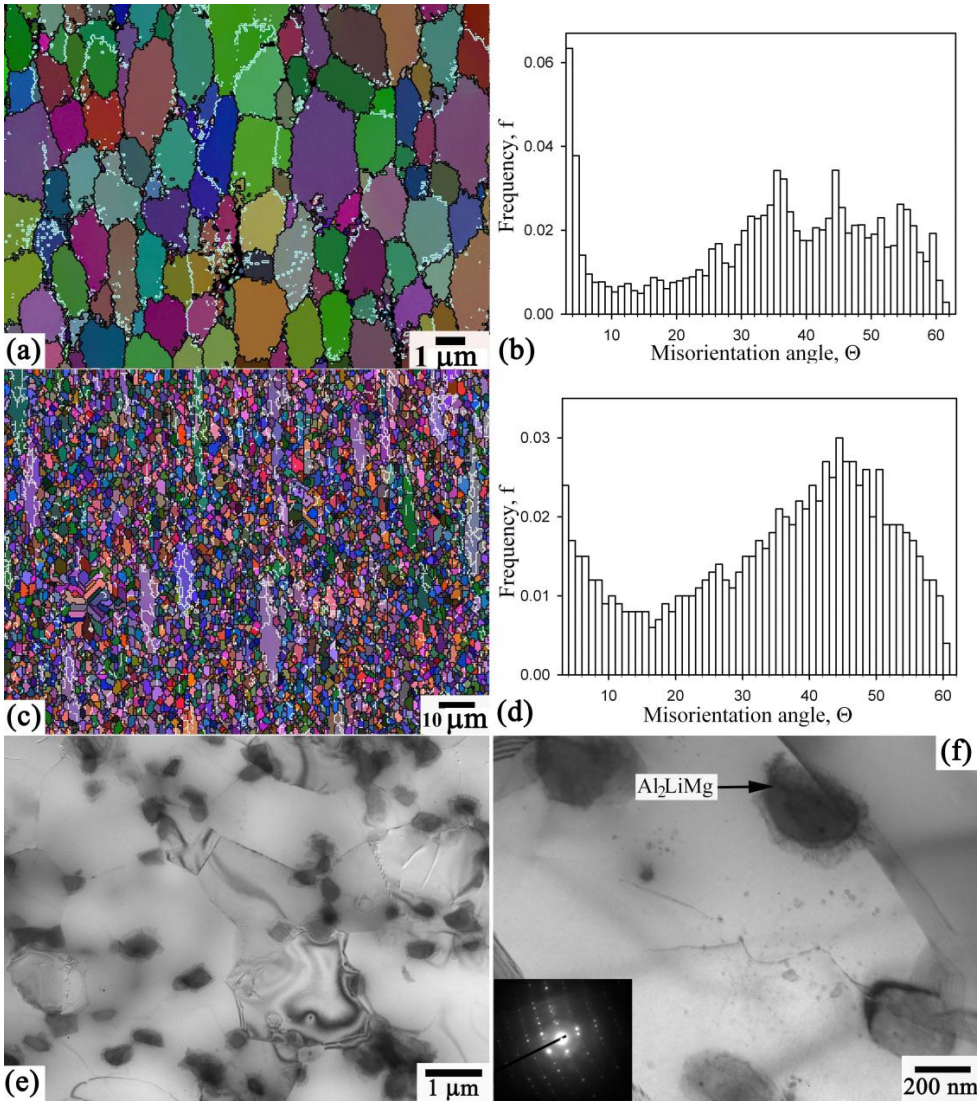

Figure 5. (**a**,**c**) Electron back scattering diffraction maps showing the high and low angle boundaries (dark and light lines, respectively) and boundary misorientation histograms (**b**,**d**) for the 1421Al alloy deformed by equal-channel angular pressing to strains of (**a**,**b**) 4; (**c**,**d**) 4 and standard heat treatment; and (**e**,**f**) transmission electron microscope image of structure ε~4 and standard heat treatment.

After ε~8, the volume fraction of grains is approximately 85%, the population of HAGBs is ~72%, the average misorientation is ~29°, and the volume fraction of the S_1-phase is ~18% (Figure 6). Most of the crystallites are grains containing low density of lattice dislocations (ρ~2 $\times$ 10^{13} m^{-2}) (Figure 6c).

Dimensions of grains and (sub)grains are essentially the same (1.4 μm, *AR*~1.2). The structures after ε~4 and ε~8 are distinctly distinguished by distribution and size of the S_1-phase (Figure 6c). Particles of this phase have an average size of ~0.8 μm. They are uniformly distributed within the aluminum matrix located both on HAGBs and within grain interiors as well (Figure 6c). As a result, this structure can be considered to be a duplex one. Dispersion of the δ′-phase was not found within grains (Figure 6c). Thus, this structure is characterized by low dislocation density, fine grains and lack of δ′-phase dispersoids within crystallites.

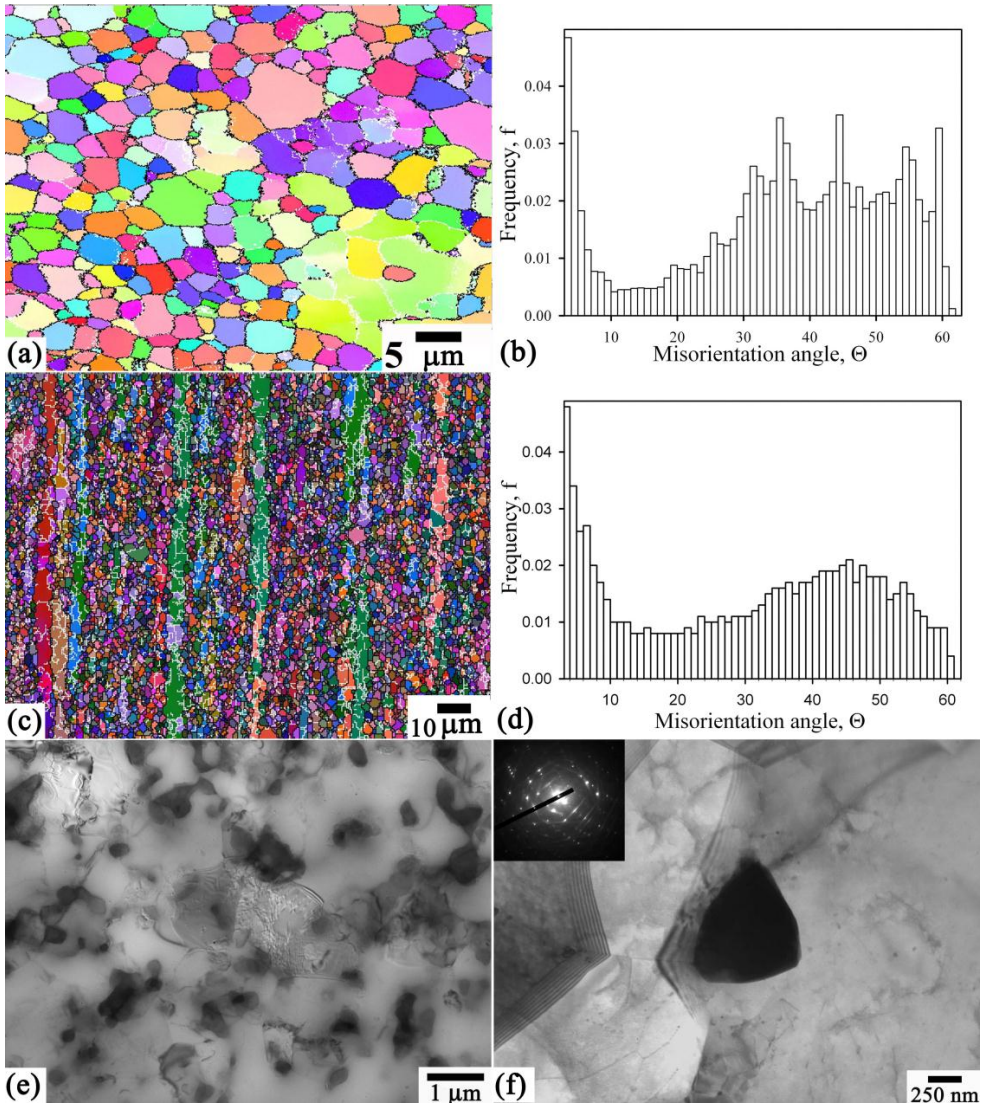

Figure 6. (**a**,**c**) Electron back scattering diffraction maps showing the high and low angle boundaries (dark and light lines, respectively) and boundary misorientation histograms (**b**,**d**) for the 1421 alloy deformed by equal-channel angular pressing to strains of (**a**,**b**) 8; (**c**,**d**) 8 and standard heat treatment; and (**e**,**f**) transmission electron microscope image of structure ε~8 and standard heat treatment.

3.4. Mechanical Properties

Figure 7a shows the engineering stress-strain curves of the 1421Al in the as-received state and after ECAP subjected to final T6 heat treatment. Values of YS, ultimate tensile strength (UTS), total elongation and uniform elongation assessed from the strain-stress curves in Figure 7a are summarized in Table 1. It is clear that the shapes of the σ-ε curves for all states of the 1421Al are similar. Extensive strain hardening takes place after reaching a yield stress. As a result, uniform elongation occurs up to

failure providing total elongation higher than 10% for all samples subjected to ECAP with different strains. It is worth noting that this type of σ-ε curves is attributed to materials with a grain size close to 1 μm having low dislocation density ($\rho < 10^{14}$ m^{-2}) and no residual stress. The values of ductility obtained can be considered sufficient [31] for Al-Li-Mg alloys. It is possible to conclude that only the T6 heat treatment following ECAP (Figure 1c) provides moderate ductility associated with significant strain hardening [24]; values of uniform elongation and elongation-to-failure are almost the same.

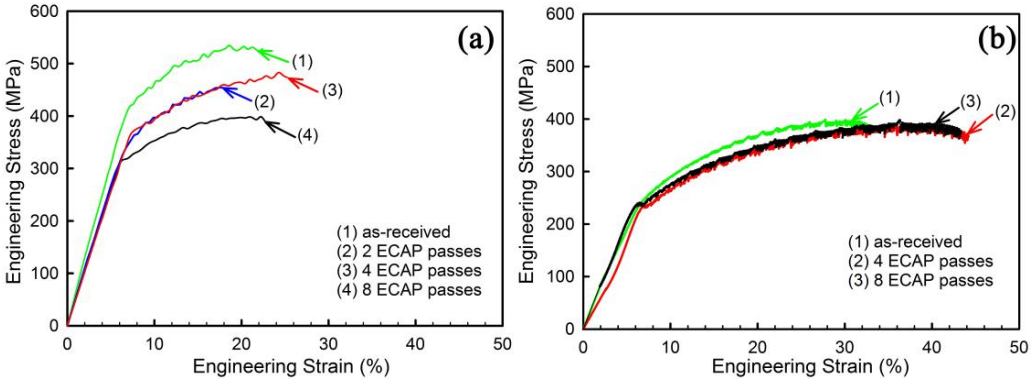

Figure 7. The engineering stress-strain curves of the 1421Al alloy at room temperature: (**a**) without and (**b**) with standard heat treatment.

Table 1. Yield stress (YS, MPa), ultimate tensile strength (UTS, MPa), ductility (δ, %) and uniform elongation (e_u, %) of the 1421Al alloy subjected to T6 heat treatment.

Conditions	YS	UTS	YS/UTS	δ	e_u
As-received	400	522	0.76	14.3	13.5
2 ECAP passes	329	480	0.68	11.3	11.3
4 ECAP passes	378	490	0.77	13.1	12
8 ECAP passes	322	451	0.71	15	15

It is observed that ECAP results in decreased yield stress and ultimate strength in the heat treated state in comparison with conventional extrusion. The 1421Al in the as-received condition exhibits the highest YS and UTS (Table 1). ECAP with a total strain of ~4 provides 6% decreases in YS and UTS (Table 1). The YS decrease is 21% and the UTS decrease is 8% in the material subjected to ECAP with a total strain of ~2 (Table 1). The effect of ECAP with a total strain of ~8 on YS is almost the same; the UTS decrease is 14% (Table 1). Thus ECAP processing of the 1421Al through the fourth route of TMP leads to minor degradation in strength; ductility remains almost unchanged. It is worth noting that the value of YS/UTS for all states of the 1421Al is close to 0.6 (Table 2) that is typical for natural aging of age-hardenable aluminum alloys if the formation of GP zones takes place.

Table 2. Yield stress (YS, MPa), ultimate strength (UTS, MPa), ductility (δ, %) and uniform elongation (e_u, %) of the 1421Al alloy without heat treatment.

Conditions	YS	UTS	YS/UTS	δ	e_u
As-received	241	398	0.6	19	17
4 ECAP passes	228	388	0.59	35	34
8 ECAP passes	226	397	0.57	29	28

Microstructural observations of the samples strained up to failure showed that there exist two types of crack initiation. In the samples subjected to ECAP with ε~2, the crack nucleation occurs in the vicinity of coarse S_1-phase particles comprising chains (Figure 8a). As a result, an interlinkage

of cracks easily occurs resulting in premature fracture. In the samples subjected to ECAP with ε~4, most of the coarse S_1-phase particles dissolved and separate particles of this phase are distributed uniformly in the aluminum matrix. Crack nucleation occurs in the vicinity of these particles (Figure 8b) or primary precipitations of Al_3(Sc,Zr)-phase (Figure 8c). However, no crack interlinkage takes place (Figure 8b,c); this material exhibits increased ductility.

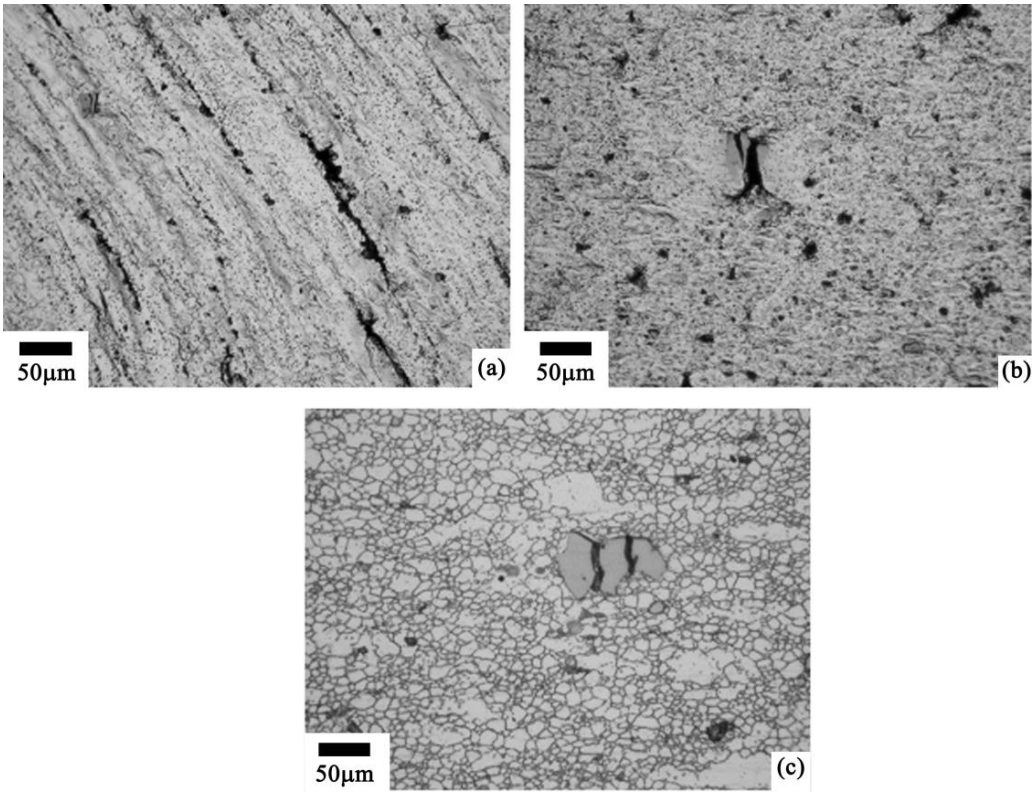

Figure 8. Typical microstructures of the samples strained up to failure: (**a**) after equal-channel angular pressing (ECAP) with ε~2; and (**b**,**c**) after ECAP with ε~ 4.

Figure 7b shows the engineering stress-strain curves of the 1421Al without heat treatment, and values of YS, UTS, total elongation and uniform elongation are presented in Table 2. All of the curves essentially have a similar shape; extensive strain hardening takes place up to failure. The serrated flow is manifested as the repeating oscillations on the stress-strain curves (Figure 7b). This phenomenon is generally associated with the Portevin-Le Chatelier (PLC) effect attributed to dynamic strain aging [29]. Characteristics of strength are almost the same for all states of the 1421Al (Table 2). However, ECAP provides 100% increases in ductility. Thus, the difference in YS and UTS between different states of the 1421Al associates mainly with differences in precipitation behavior. Notably, the value of YS/UTS for all states of the 1421Al is close to 0.75 (Table 1), which is typical for artificial aging of age-hardenable aluminum alloys if the formation of nanoscale dispersoids with coherent interface boundaries takes place.

4. Discussion

It is observed that the deformed structure developed in the 1421Al containing coherent Al3Sc dispersoids under ECAP is retained under solution treatment. The Al_3Sc nanoscale particles are very effective in pinning HAGBs and LAGBs, suppressing recrystallization and recovery processes at 460 °C. Therefore, the fourth route of TMP is suitable for application to this alloy. However, ECAP provided no positive influence on mechanical properties. This fact is caused by a strong effect of UFG on aging response in Al-Li-Mg alloys.

It is apparent that the 1421Al with different types of deformation structures without heat treatment shows essentially similar strength due to dynamic strain aging. It is known [36] that jerky flow can be associated with the formation of clouds of solutes around the dislocations (normal PLC) or precipitations of coherent dispersoids on dislocation (pseudo-PLC). The origin of PLS effect was not examined in this study. However, it is assumed that the appearance of jerky flow is attributed to precipitation of the δ′-phase on dislocations [16]. As a result, dislocations become immobile, and LAGBs with misorientation higher than 6° start to play a role of effective barrier for gliding dislocation. In this case, the subgrains with the LAGBs can be considered as grains in the Hall-Petch equation, which states that the YS, σ_y, is given by

$$\sigma_y = \sigma_0 + k_y d^{-1/2} \quad (2)$$

where σ_0 is termed the friction stress and k_y is a constant of yielding [1]. However, subgrain structure as well as UFG structure provide nearly the same grain size strengthening in accordance with Equation (2). Perhaps this is why the YS values for 1421Al with well-defined subgrain structure, partially recrystallized structure and fully recrystallized structure are almost the same in initial condition without heat treatment. The difference in the YS arises due to heat treatment.

After heat treatment, no jerky flow was observed in all states of the 1421Al because all Li precipitated in the form of different phases indicated in the first scheme (Figure 1a). In an extruded bar of the 1421Al, the precipitation sequence is described by Equation (1). As a result, at 120 °C, the precipitation of nanoscale particles of coherent δ′-phase provides extensive dispersion strengthening. δ′-phase free zones are evolved only in the vicinity of coarse S_1-phase particles. The last phase is a stable phase in comparison with the δ′-phase. As a result, under any aging conditions, the δ′-phase dispersoids will be dissolved around HAGBs where stable S_1-phase nucleates. The rate of this process is dependent on diffusion path, and, therefore, aging temperature and distribution of S_1-phase particles within aluminum matrix will strongly affect this process.

The S_1-phase tends to precipitate in a strong heterogeneous manner on HAGBs. As a result, in the 1421Al subjected to ECAP with ε~4, the S_1-phase precipitates uniformly on boundaries of micron scale grains. Diffusion path is very short and almost all dispersoids of the δ′-phase dissolve under aging even at low temperature. In this state of the 1421Al, the dispersion strengthening associated with the S_1-phase plays an unimportant role in the strength of this alloy; particles of this phase are relatively coarse, and, in addition, most of them are located on HAGBs. As a result, these particles are not able to impede dislocation motion. The heat treatment provides a 62% increase in YS; however, the origin of this increase is unknown. We can assume only that S_1-phase particles may hinder operation of grain boundary dislocation sources, and sparse dispersoids of the δ′-phase effectively impede dislocation glide within micron scale grains. It is worth noting that the value of YS/UTS~0.76 (Table 1) for this state of the 1421Al and for the hot extruded state is almost the same despite significant differences in origin and distribution of secondary phases.

The formation of coarser particles of the S_1-phase in the 1421Al subjected to ECAP with ε~8 provides a 42% increase in YS. Extensive localization of plastic deformation resulting in cracking along the chains of coarse S_1-phase particles takes place in the 1421Al subjected to ECAP with ε~2. This localization occurs within the δ′-phase free zones around the S_1-phase particles. As a result, the heat treatment provides a 44% increase in YS that is significantly less than that (66%) for the hot extruded state of the 1421Al.

Thus, to achieve a positive effect from extensive grain refinement by ECAP on the strength of age-hardenable aluminum alloys, it is necessary to modify chemical composition and aging regimes to prevent the formation of stable phases on HAGBs undergoing final heat treatment.

5. Conclusions

It was shown that the post-ECAP standard heat treatment consisting of solution treatment, quenching and final aging can be applied to the 1421Al with different types of deformation structures

including an ultra-fine grained structure produced by ECAP. It was found that deformation structures evolved during ECAP processing are stable under solution treatment. However, aging of the 1421Al with these structures is not capable of providing significant precipitation hardening. The formation of coarse particles of the stable S1-phase on boundaries of micron scale grains and even within interiors of these grains prevents the precipitation of nanoscale dispersoids of the δ'-phase under aging conditions that leads to a decrease in strength of the alloy.

Acknowledgments: The financial support received from the Ministry of Education and Science, Moscow, Russia, (Belgorod State University project No. 14.587.21.0018 (RFMEFI58715X0018)) is acknowledged. The main results were obtained by using equipment from the Joint Research Center, Belgorod State University.

Author Contributions: A.M. and R.K. conceived and designed the experiments; A.M. performed the experiments. A.M. and R.K. discussed and analyzed the obtained results.

Conflicts of Interest: The authors declare no conflict of interest.

References

1. Valiev, R.Z.; Langdon, T.G. Principles of equal-channel angular pressing as a processing a processing tool for grain refinement. *Prog. Mater. Sci.* **2006**, *51*, 881–981. [CrossRef]
2. Kaibyshev, R.; Tagirov, D.; Mogucheva, A. Cost-Affordable Technique Involving Equal Channel Angular Pressing for the Manufacturing of Ultrafine Grained Sheets of an Al-Li-Mg-Sc Alloy. *Adv. Eng. Mater.* **2010**, *12*, 735–739. [CrossRef]
3. Ferrasse, S.; Segal, V.M.; Alford, F.; Kardokus, J.; Strothers, S. Scale up and application of equal-channel angular extrusion for the electronics and aerospace industries. *Mater. Sci. Eng. A* **2008**, *493*, 130–140. [CrossRef]
4. Yuzbekova, D.; Mogucheva, A.; Kaibyshev, R. Superplasticity of ultrafine-grained Al-Mg-Sc-Zr alloy. *Mater. Sci. Eng. A.* **2016**, *675*, 228–242. [CrossRef]
5. Murayama, M.; Horita, Z.; Hono, K. Microstructure of two-phase Al-1.7 at. % Cu alloy deformed by equal-channel angular pressing. *Acta Mater.* **2001**, *49*, 21–29. [CrossRef]
6. Radetic, T.; Popovic, M.; Romhanji, E.; Verlinden, B. The effect of ECAP and Cu addition on the aging response and grain substructure evolution in an Al-4.4 wt. % Mg alloy. *Mater. Sci. Eng. A* **2010**, *527*, 634–644. [CrossRef]
7. Kim, J.K.; Kim, H.K.; Park, J.W.; Kim, W.J. Large enhancement in mechanical properties of the 6061 Al alloys after a single pressing by ECAP. *Scr. Mater.* **2005**, *53*, 1207–1211. [CrossRef]
8. Kim, W.J.; Wang, J.Y. Microstructure of the post-ECAP aging processed 6061 Al alloys. *Mater. Sci. Eng. A* **2007**, *464*, 23–27. [CrossRef]
9. Kim, W.J.; Chung, C.S.; Ma, D.S.; Hong, S.I.; Kim, H.K. Optimization of strength and ductility of 2024 Al by equal channel angular pressing (ECAP) and post-ECAP aging. *Scr. Mater.* **2003**, *49*, 333–338. [CrossRef]
10. Shaterani, P.; Zarei-Hanzaki, A.; Fatemi-Varzaneh, S.M.; Hassas-Irani, S.B. The second phase particles and mechanical properties of 2124 aluminum alloy processed by accumulative back extrusion. *Mater. Des.* **2014**, *58*, 535–542. [CrossRef]
11. Cabibbo, M. Partial dissolution of strengthening particles induced by equal channel angular pressing in an Al-Li-Cu alloy. *Mater. Charact.* **2012**, *68*, 7–13. [CrossRef]
12. Namdar, M.; Jahromi, S.A.J. Influence of ECAP on the fatigue behavior of age-hardenable 2xxx aluminum alloy. *Int. J. Miner. Metall. Mater.* **2015**, *22*, 285–291. [CrossRef]
13. Kotan, G.; Tan, E.; Kalay, Y.E.; Gür, C.H. Homogenization of ECAPed Al 2024 alloy through age-hardening. *Mater. Sci. Eng. A* **2013**, *559*, 601–606. [CrossRef]
14. Roshan, M.R.; Jahromi, S.A.J.; Ebrahimi, R. Predicting the critical pre-aging time in ECAP processing of age-hardenable aluminum alloys. *J. Alloy. Compd.* **2011**, *509*, 7833–7839. [CrossRef]
15. Shaeri, M.H.; Shaeri, M.; Ebrahimi, M.; Salehi, M.T.; Seyyedein, S.H. Effect of ECAP temperature on microstructure and mechanical properties of Al-Zn-Mg-Cu alloy. *Prog. Nat. Sci. Mater. Int.* **2016**, *26*, 182–191. [CrossRef]

16. Salem, H.G.; Goforth, R.E.; Hartwig, K.T. Influence of intense plastic straining on grain refinement, precipitation, and mechanical properties of Al-Cu-Li-based alloys. *Metall. Mater. Trans.* **2003**, *34A*, 1153–1161. [CrossRef]
17. Zhao, Y.H.; Liao, X.Z.; Jin, Z.; Valiev, R.Z.; Zhu, Y.T. Microstructures and mechanical properties of ultrafine grained 7075 Al alloy processed by ECAP and their evolutions during annealing. *Acta Mater.* **2004**, *52*, 4589–4599. [CrossRef]
18. Mohamed, I.F.; Yonenaga, Y.; Lee, S.; Edalati, K.; Horita, Z. Age hardening and thermal stability of Al-Cu alloy processed by high-pressure torsion. *Mater. Sci. Eng. A* **2015**, *627*, 111–118. [CrossRef]
19. Kim, W.J.; Kim, J.K.; Kim, H.K.; Park, J.W.; Jeong, Y.H. Effect of post equal-channel-angular-pressing aging on the modified 7075 Al alloy containing Sc. *J. Alloy. Compd.* **2008**, *450*, 222–228. [CrossRef]
20. Hirosawa, S.; Hamaoka, T.; Horita, Z.; Lee, S.; Matsuda, K.; Terada, D. Methods for Designing Concurrently Strengthened Severely Deformed Age-Hardenable Aluminum Alloys by Ultrafine-Grained and Precipitation Hardenings. *Metall. Mater. Trans. A* **2013**, *44A*, 3921–3933. [CrossRef]
21. Roven, H.J.; Nesboe, H.; Werenskiold, J.C.; Seibert, T. Mechanical properties of aluminium alloys processed by SPD: Comparison of different alloy systems and possible product areas. *Mater. Sci. Eng. A* **2005**, *410–411*, 426–429. [CrossRef]
22. Mallikarjuna, C.; Shashidhara, S.M.; Mallik, U.S. Evaluation of grain refinement and variation in mechanical properties of equal-channel angular pressed 2014 aluminum alloy. *Mater. Des.* **2009**, *30*, 1638–1642. [CrossRef]
23. Sabirov, I.; Estrin, Y.; Barnett, M.R.; Timokhina, I.; Hodgson, P.D. Enhanced tensile ductility of an ultra-fine-grained aluminum alloy. *Scr. Mater.* **2008**, *58*, 163–166. [CrossRef]
24. Valiev, R.Z.; Murashkin, M.Y.; Bobruk, E.V.; Raab, G.I. Grain refinement and mechanical behavior of the Al Alloy, subjected to the new SPD technique. *Mater. Trans.* **2009**, *50*, 87–91. [CrossRef]
25. Chinh, N.Q.; Gubicza, J.; Czeppe, T.; Lendvai, J.; Xu, C.; Valiev, R.Z.; Langdon, T.G. Developing a strategy for the processing of age-hardenable alloys by ECAP at room temperature. *Mater. Sci. Eng. A* **2009**, *516*, 248–252. [CrossRef]
26. Kim, J.K.; Jeong, H.G.; Hong, S.I.; Kim, Y.S.; Kim, W.J. Effect of aging treatment on heavily deformed microstructure of a 6061 aluminum alloy after equal channel angular pressing. *Scr. Mater.* **2001**, *45*, 901–907. [CrossRef]
27. Kim, W.J.; Kim, J.K.; Park, T.Y.; Hong, S.I.; Kim, D.I.; Kim, Y.S.; Lee, J.D. Enhancement of strength and superplasticity in a 6061 Al alloy processed by equal-channel-angular-pressing. *Metall. Mater. Trans. A* **2002**, *33*, 3155–3164. [CrossRef]
28. Wang, Z.C.; Prangnell, P.B. Microstructure refinement and mechanical properties of severely deformed Al-Mg-Li alloys. *Mater. Sci. Eng A* **2002**, *328*, 87–97. [CrossRef]
29. Kaibyshev, R.; Shipilova, K.; Musin, F.; Motohashi, Y. Continuous dynamic recrystallization in an Al-Li-Mg-Sc alloy during equal-channel angular extrusion. *Mater. Sci. Eng.* **2005**, *21*, 408–418. [CrossRef]
30. Musin, F.; Kaibyshev, R.; Motohashi, Y.; Sakuma, T.; Itoh, G. High strain rate superplasticity in an Al-Li-Mg alloy subjected to equal-channel angular extrusion. *Mater. Trans.* **2002**, *43*, 2370–2377. [CrossRef]
31. Kaibyshev, R.; Shipilova, K.; Musin, F.; Motohashi, Y. Continuous dynamic recrystallization in an Al-Li-Mg-Sc alloy during equal-channel angular extrusion. *Mater. Sci. Eng. A* **2005**, *396*, 341–351. [CrossRef]
32. Mogucheva, A.A.; Kaibyshev, R.O. Structure and properties of aluminum alloy 1421 after equal-channel angular pressing and isothermal rolling. *Phys. Met. Metall.* **2008**, *106*, 424–433. [CrossRef]
33. Fridlyander, I.N.; Chuistova, K.V.; Berezina, A.L.; Kolobnev, N.I. *Aluminum–Lithium Alloys. Structure and Properties*; Naukova Dumka: Kiev, Ukraine, 1992; p. 192.
34. Lee, S.; Berbon, P.B.; Furukawa, M.; Horita, Z.; Nemoto, M.; Tsenev, N.K.; Valiev, R.Z.; Langdon, T.G. Developing superplastic properties in an aluminum alloy through severe plastic deformation. *Mater. Sci. Eng. A* **1999**, *272*, 63–72. [CrossRef]
35. Kaibyshev, O.A. *Superplasticity of Alloys, Intermetallics, and Ceramics*; Springer: Berlin, Germany, 1992; p. 149.
36. Brechet, Y.; Estrin, Y. On the influence of precipitation on the Portevin-Le Chatelier effect. *Acta Metall. Mater.* **1995**, *43*, 955–963. [CrossRef]

© 2016 by the authors; licensee MDPI, Basel, Switzerland. This article is an open access article distributed under the terms and conditions of the Creative Commons Attribution (CC-BY) license (http://creativecommons.org/licenses/by/4.0/).